# Insights into Tyrosine Phosphorylation Control of Protein−Protein Association from the NMR Structure of a Band 3 Peptide Inhibitor Bound to Glyceraldehyde-3-phosphate Dehydrogenase[†,‡]

Elan Zohar Eisenmesser[§] and Carol Beth Post*[,||]

*Department of Biological Sciences, Purdue University, West Lafayette, Indiana 47907-1392, and Department of Medicinal Chemistry, Purdue University, West Lafayette, Indiana 47907-1333*

*Received June 17, 1997; Revised Manuscript Received September 3, 1997*[⊗]

ABSTRACT: A protein−protein association regulated by phosphorylation of tyrosine is examined by NMR structural studies and biochemical studies. Binding of glyceraldehyde-3-phosphate dehydrogenase (G3PDH) and aldolase to the N-terminus of human erythrocyte anion transporter, band 3, inhibits enzyme activity. This inhibition is reversed upon phosphorylation of band 3 Y8, as shown by kinetic studies on purified components, as well as *in vivo* studies. Thus, tyrosine phosphorylation mediates *against* the intermolecular protein−protein association, in contrast to the positive control involving SH2 and PTB domains where phosphorylation is required for binding. To elucidate the basis of recognition and negative control by tyrosine phosphorylation, the structure of a synthetic peptide, B3P, corresponding to the first 15 residues of band 3 (MEELQDDYEDMMEEN-$NH_2$), bound to G3PDH has been determined using the exchange-transferred nuclear Overhauser effect. The G3PDH-bound B3P structure was found to be very similar to the structure recognized by aldolase. A hydrophobic triad forms from side chains within a loop structure of residues 4 through 9 in both bound species. Another structural feature stabilizing the loop, in the case of the B3P−G3PDH complex, is a hydrogen bond between the side chains of Y8 and D10 associated with a $\beta$-turn of residues 8−11. Based on the structure of this *p*hosphorylation *s*ensitive *i*nteraction (PSI) loop, it is suggested that tyrosine phosphorylation disrupts protein−protein association, in part, by intramolecular electrostatic destabilization. The inhibition by B3P is competitive with respect to the coenzyme $NAD^+$ and noncompetitive with the substrate analog arsenate. Specific binding of B3P to G3PDH is demonstrated by reversion of the NMR spectral properties of bound B3P to those of the free peptide upon addition of coenzyme and substrate analog. The stoichiometry of binding for the B3P−G3PDH complex was determined from Sephadex G-50 displacement experiments to be 4:1. Collectively, these results are consistent with B3P binding the active site of G3PDH.

Phosphorylation of tyrosine regulates the formation of protein−protein complexes both in the initial and in the downstream steps of signal transduction pathways. The phosphorylated form of tyrosine is required for binding to SH2 and phosphotyrosine binding (PTB)[1] domains in the regulation of protein kinase activity. Alternatively, phosphorylation can mediate *against* protein association, as in the case of band 3, the erythrocyte anion transporter. Band 3 is a substrate of $p72^{syk}$ tyrosine kinase (Harrison et al., 1994). In its unphosphorylated form, band 3 binds and inhibits the enzymatic activity of aldolase, phosphofructokinase (PFK), and glyceraldehyde-3-phosphate dehydrogenase (G3PDH) (Low, 1986). Phosphorylation reverses binding and inhibition of glycolytic enzymes, as shown by *in vitro* kinetic studies (Low et al., 1987). Further, the addition of compounds that promote phosphorylation of band 3 to resealed erythrocytes increases glycolysis in a manner related to the release of glycolytic enzymes from band 3 (Harrison et al., 1991). Structural studies related to complexes under positive control by phosphorylation have been critical for understanding these protein−protein associations (Hubbard

[†] This work was supported by a grant to C.B.P. from the NIH (R01-GM39478). C.B.P. was supported by a Research Career Development Award from the NIH (K04-GM00661), and E.Z.E. received a training fellowship from the NIH (5T32-GM08296). The NMR and peptide synthesis facilities are supported by a grant to the Purdue Cancer Center. The computing facilities shared by the Structural Biology group were supported by grants from the Lucille P. Markey Foundation and the Purdue University Academic Reinvestment Program.

[‡] The atomic coordinates have been deposited in the Brookhaven Protein Data Bank (Accession Number 3BTB).

* To whom correspondence should be addressed.

[§] Department of Biological Sciences.

[||] Department of Medicinal Chemistry.

[⊗] Abstract published in *Advance ACS Abstracts,* November 1, 1997.

[1] Abbreviations: G3PDH, glyceraldehyde-3-phosphate dehydrogenase; PFK, phosphofructokinase; $NAD^+$, nicotinamide adenine dinucleotide; NADH, reduced form of nicotinamide adenine dinucleotide; syk, spleen tyrosine kinase; B3P, band 3 peptide; ET-NOESY, exchange-transferred nuclear Overhauser effect spectroscopy; *t*-BOC, *tert*-butyloxycarbonyl; FMOC, 9-fluorenylmethyloxycarbonyl; HPLC, high-performance liquid chromatography; FPLC, fast-performance liquid chromatography; TFA, trifluoroacetic acid; ssNOESY, symmetrically shifted nuclear Overhauser effect spectroscopy; MD, molecular dynamics; SA, simulated annealing; SH, *src* homology region, PTB, phosphotyrosine binding; PSI, phosphorylation sensitive interaction.

S0006-2960(97)01445-1 CCC: $15.00 
Published on Web 01/20/1998

et al., 1994; Andreotti et al., 1997; Xu et al., 1997; Sicheri et al., 1997). Here, we report NMR and biochemical studies that examine the structural features of the band 3 interaction with G3PDH, a complex under negative control by tyrosine phosphorylation.

Erythrocytes exhibit a high level of protein tyrosine kinase activity (Tuy et al., 1983) even though these cells are terminally differentiated and do not undergo cell division. In spite of the curious presence of kinase activity, the basis for triggering this activity remains unknown. It has been shown that band 3 is the major tyrosine-phosphorylated protein (Tuy et al., 1983, 1985; Harrison et al., 1994). Investigations with red cell membrane ghosts purified in the presence of $p72^{syk}$ show Y8 to be the most readily phosphorylated residue (Dekowski et al., 1983; Yannoukakos et al., 1991). A series of studies has lead to the suggestion that tyrosine phosphorylation control of the association of band 3 with glycolytic enzymes forms part of a regulatory scheme for red cell metabolism (Low et al., 1987, 1993; Harrison et al., 1991).

With approximately one million copies per erythrocyte and a molecular mass of 93 000 daltons, band 3 protein makes up roughly 25% of human erythrocyte membrane protein (Low, 1986), and functions to exchange chloride for bicarbonate anion. As indicated above, band 3 may also function in the regulation of red cell metabolism. High-affinity binding sites for glycolytic enzymes are present on the acidic N-terminus region of band 3 (Low, 1986), and binding has been shown to have reversible inhibitory effects on enzymatic activity (Murthy et al., 1981; Tsai et al., 1981). G3PDH preferentially binds to residues 1−11, while aldolase binds to both residues 1−11 and 13−31 (Low, 1986; Kaul et al., 1983). Further, direct observation finds the majority of G3PDH in red blood cells to be associated with the membrane (Rogalski et al., 1989), and glycolytic levels in the red blood cell can be altered 30-fold by modulating the interaction between band 3 and the glycolytic enzymes (Low et al., 1993). These results collectively support a mechanism for controlling red cell metabolism via the band 3−glycolytic enzyme association.

In an initial approach to defining structural features of a complex involving an integral membrane protein and a soluble one, the three-dimensional structure of a pentadecameric peptide derived from the N-terminus of band 3 (B3P) when it is bound to G3PDH was determined using interproton distances interpreted from exchange-transferred nuclear Overhauser effect data (Balaram et al., 1973; Clore et al., 1982, 1983; Campbell & Sykes, 1993; Ni, 1994; Murali et al., 1994). These investigations were motivated in part by the question of whether the structure of band 3 recognized by G3PDH is similar to that recognized by aldolase. Earlier studies on the B3P−aldolase complex determined the aldolase-bound structure of B3P to be a loop conformation which folds around the tyrosine side chain and is stabilized by nonpolar interactions of the triad L4, Y8, and M12 (Schneider & Post, 1995). Based on this *p*hosphorylation *s*ensitive *i*nteraction (PSI) loop conformation, it was proposed that the mechanism by which phosphorylation diminishes protein−protein association is destabilization of this loop structure by intramolecular electrostatic repulsion. Results reported here show that a similar loop conformation is recognized by G3PDH, suggesting that the PSI−loop mechanism may have a general role in the negative control of protein−protein interactions.

The aims of this paper are to elucidate the binding of B3P to G3PDH and inhibition of enzyme activity, and to further characterize the role of the PSI loop in mediating protein−protein association.

## MATERIALS AND METHODS

*Peptide and Enzyme Preparation.* The band 3 peptide (MEELQDDYEDMMEEN-$NH_2$) was synthesized by the Purdue University Peptide Synthesis Facility and further purified as described in Schneider and Post (1995). Both *t*-BOC and FMOC amino acid derivatives were used. Briefly, a Pharmacia preparatory column (25 mm × 15 cm, $C_2$−$C_{18}$, 15 $\mu$m silica particle size) was used for separation with a solvent system of 0.1% TFA in 95% $H_2O$/5% HPLC-grade acetonitrile and 0.1% TFA in 5% $H_2O$/95% HPLC-grade acetonitrile.

G3PDH was purchased as a crystalline suspension and concanavalin A as a lyophilized powder, both from Worthington. Unless otherwise noted, enzymes were dialyzed overnight in 5 mM imidazole/4 mM sodium acetate at pH 7.5 and 4 °C. Concentrations were checked at 276 nm for G3PDH [$\epsilon$ =1.053 mL $mg^{-1}$ $cm^{-1}$ (Worthington Enzymes, 1996)] and at 280 nm for concanavalin A [$\epsilon$ = 1.056 mL $mg^{-1}$ $cm^{-1}$ (Worthington Enzymes, 1996)] using a Perkin Elmer Lambda 6 UV/Vis spectrometer.

*Enzyme Kinetics.* Initial velocity measurements, following NADH production at 340 nm, were conducted on G3PDH with either $NAD^+$ (Boehringer Mannheim GmbH) or arsenate (J. T. Baker Chemical Co.) as variable substrates, and the inhibitor B3P at concentrations of 0.0, 0.05, and 0.10 mM. Arsenate was used in place of phosphate to prevent product inhibition; the product, 1-arsenate-3-phosphoglycerate, is unstable and hydrolyzes to 3-phosphoglycerate and arsenate (Orsi & Cleland, 1972). A 1.5 mL cuvette with a path length of 1 cm was used for all UV measurements. Conditions for kinetic measurements were 10 mM imidazole and 8 mM sodium acetate at pH 7.5 and 25 °C. G3PDH was dialyzed overnight at 4 °C in the same buffer. The components, $4.26 \times 10^{-7}$ M G3PDH, 0.1 mM dithiothreitol (Sigma), 0.1 mM $NAD^+$ or arsenate, and 0.025−0.100 mM arsenate or $NAD^+$, respectively, were placed into the cuvette and the reaction was initiated with the addition of 0.1 mM G3P (Sigma). Initial velocities were obtained from the absorbance change over the first 10 s only, since G3P is unstable in solution (Duggleby & Dennis, 1974). The kinetic constants were found with the least-squares fitting program Kinetics (Cleland, 1979).

*Sephadex G-50 Displacement Chromatography.* Sephadex G-50 columns were prepared from beads washed 3 times in 1.0 mM imidazole at pH 7.0 and left in the same buffer overnight, and then poured into a 1 $cm^3$ syringe. Columns were first spun for 2 min to remove excess buffer, and no peptide was detected in the flow-through when placed, in the absence of enzyme, onto the Sephadex G-50 column. Varying concentrations of B3P, from 0.04 to 4.52 mM, were added to 0.15 mM G3PDH in 1.0 mM imidazole at pH 7.0 and 4 °C; 100 $\mu$L volumes were placed onto the Sephadex G-50 column, and the column was spun in an IEC Clinical Centrifuge at level 4, approximately 495*g*, for 2 min.

Collected fractions were then analyzed for their G3PDH and B3P content. Displacement of a single column volume yields only the B3P−G3PDH complex since the mobility of free B3P through the column is significantly less than that of the complex. G3PDH concentrations were determined from absorbance at 276 nm and not corrected for the relatively small B3P absorption. B3P was separated by FPLC with a Pharmacia pepRPC HR 5/5 analytical column (C2−C18, 5 $\mu$m silica particle size) using the solvent system described above. B3P concentrations were determined from peak heights of 210 nm absorbance and standards constructed with B3P to relate peak heights to concentration. A total of 15 data points were collected in triplicate over the course of 4 preparations of this experiment, and the standards were recalibrated each time.

Rabbit muscle G3PDH as received from Worthington is known to contain at least one coenzyme per tetramer (Vijlder & Slater, 1968; Fox & Dandliker, 1956). The affinity of coenzyme binding the first site on G3PDH is about 10 nM (Meunier & Dalziel, 1977). Thus, some samples for displacement chromatography were purified further by charcoal treatment. Dialyzed enzyme was added to 1.0% charcoal (Norit SX2) and stirred in 1.0 mM imidazole at pH 7.0 at 4 °C for approximately 20 min. The charcoal was separated from soluble enzyme by low-speed centrifugation and the enzyme solution concentrated 2−3 fold. After repeating this procedure twice, the measured $A_{280}$:$A_{260}$ ratio was 1.62, equivalent to approximately 0.50−0.72 mol of coenzyme per tetramer (Vijlder & Slater, 1968; Fox & Dandliker, 1956) still present. Further charcoal treatment was not found to remove significant amounts of coenzyme and led to substantial loss of enzymatic activity. The Sephadex G-50 displacement assay was repeated 5 times with 0.16 mM charcoal-treated G3PDH and 4.52 mM B3P.

*Sample Preparation and NMR Spectroscopy.* Samples were pH adjusted in $H_2O$ and lyophilized for solvent exchange. They were placed into 5 mm NMR tubes with 0.8 mL of either 99.96% $D_2O$ (Isotec, Inc.) or 85% $H_2O$/15% $D_2O$ with final buffer concentrations of 10 mM imidazole and 8 mM sodium acetate. Unless otherwise noted, the pH was adjusted to 7.5 where the pH meter value was not corrected for deuterium effects.

Exchanged-transferred (ET) symmetrically shifted NOESY (ssNOESY) (Clore & Gronenborn, 1982, 1983; Smallcombe, 1992) spectra were recorded at 14.1 T on a Varian UnityPlus 600 at 4 °C using an 8 mm probe with a self-shielded z-gradient coil. A symmetrically shifted pulse, with maxima set at ±2148 Hz from the transmitter, was used as the NOESY read pulse. All other $^1$H spectra, including ET-NOESY experiments in 99.96% $D_2O$, were collected on a Varian VXR-500 at 4 °C using the decoupler or transmitter channels to saturate the HDO resonance for a period of 2.5 s. All ET-NOESY spectra contained 256 hypercomplex t1 date points and 2K data points in the t2 dimension collected in the phase-sensitive mode using the method of States et al. (1982) for quadrature detection, 32 transients per t1 increment, and a 12 ppm spectral window centered at the water resonance. A mixing time of 150 ms for all 2D data was employed with a recycle time of at least 2.5 s.

VNMR 3.1 software from Varian running on a SUN Sparc 1+ workstation was used for all spectral processing. Two-dimensional spectra were zero-filled to generate 4K × 4K data sets, and the time domain data were weighted with Gaussian apodization in both dimensions.

Assignments at pH 7.5 were determined by measuring the pH dependence of the chemical shifts using previously assigned resonances at pH 5.5 (Schneider & Post, 1996). The pH of 2.5 mM B3P samples was adjusted by approximately 0.5 pH increments, from 5.5 to 7.5, in the NMR tubes with sodium deuteroxide and deuterium chloride using an ultra-thin, long-stem NMR electrode (Aldrich). For amide resonances, titrations were conducted with a 1,1-echo pulse sequence (Sklenar & Bax, 1987), to avoid saturation of water, in 85% $H_2O$/15% $D_2O$. For aliphatic resonances, titrations were conducted with a standard two-pulse sequence using the decoupler for presaturation of the HDO resonance in 99.96% $D_2O$. Several chemical shift changes were observed for the amide protons, including 0.05 ppm for N15 $H_N$ and 0.10 ppm for E14 $H_N$. The largest chemical shift observed in the aliphatic region was that of M1 $H_\alpha$, shifting approximately 0.15 ppm upfield from pH 5.5 to pH 7.5. There is considerably more overlap at pH 7.5 as compared to pH 5.5. This overlap was especially problematic among the protons M11 $H_{\gamma1,\gamma2}$, M12 $H_{\gamma1,\gamma2}$, D6 $H_{\beta1,\beta2}$, and D7 $H_{\beta1,\beta2}$, which resonate at 2.27 ppm, and meant many NOE interactions were not used for structure determination since they could not be assigned unambiguously.

*NMR Structure Determination.* Interproton distance restraints were categorized based on integrated NOESY cross-peak intensities. In the case of ET-ssNOESY spectra, observed intensities were weighted by the excitation profile calculated with the program Axum (TriMetrix, Inc) for a composite of two sinc functions with equal offsets but opposite signs (Smallcombe, 1995). Only the F2 dimension was weighted.

The cross-peak between the ring protons of Y8 was used as a reference for both the ET-ssNOESY data taken in 85% $H_2O$/15% $D_2O$ and the ET-NOESY data measured in 99.96% $D_2O$. This reference is the summed intensity for two NOE pairs ($H_{\delta1}-H_{\epsilon1}$ and $H_{\delta2}-H_{\epsilon2}$) each with a fixed interproton distance, $r$ = 2.5 Å. Other NOE intensities were categorized as strong (1.8−2.7 Å restraint), medium (1.8−3.3 Å restraint), or weak (1.8−5.0 Å restraint), assuming a $1/r^6$ dependence of the cross-peak intensity. With regard to the exchange process, setting the cross-peak intensity proportional to $1/r^6$ assumes that this process affects the intensities uniformly. At the level of accuracy of the qualitative categorization of distances, this assumption is valid in the fast exchange limit and because the differences due to variations in the free peptide $T1$ values are small at 150 ms mixing time (Zheng & Post, 1992).

Three-dimensional structures of B3P bound to G3PDH were determined using simulated annealing with two force fields and otherwise similar protocols. The first case employed X-PLOR 3.1 (Brunger, 1992) and a force field (topallhdg.pro and parallhdg.pro files) with no electrostatics, a soft square-well potential for the distance restraints, and a purely repulsive van der Waals term, $k_{vdw}(r_{min}^2 - r^2)^2$, where $k_{vdw}$ is the force constant and $r_{min}$ is the sum of the van der Waals radii between two atoms (Brunger, 1988; Kraulis et al., 1989). The second case employed CHARMM version23 (Brooks et al., 1983) and a force field (top_all22_prot.inp and par_all22_prot.inp files) (MacKerrell et al., 1992) with no electrostatics, a square-well potential for the distance

restraints, and a full Lennard−Jones potential. A force constant of 50 kcal mol$^{-1}$ Å$^{-2}$ was used for restraining distances based on NOE intensity in all molecular dynamics and energy minimization steps. Modifications to the CHARMM force field were made to ensure tyrosine ring planarity and a trans peptide bond; improper dihedrals with 500 kcal mol$^{-1}$ rad$^{-2}$ force constants were added to the tyrosine ring, and improper dihedrals with 100 kcal mol$^{-1}$ rad$^{-2}$ force constants were added to the peptide bond. To make the search of conformational space more efficient, 14 $\phi$ dihedral restraints were used in the initial stages to limit peptide structures to $-180° \leq \phi \leq -30°$, the region of a Ramachandran plot populated by nearly all non-glycyl residues. Importantly, these dihedral restraints were removed for the final steps of molecular dynamics and energy minimization and, as such, were not a determinant in the final structures. CHARMM23 was modified to incorporate a harmonic dihedral restraint function with a window. The force constant for this restraint function was 5 kcal mol$^{-1}$ rad$^{-2}$ for high-temperature dynamics, increased to 200 kcal mol$^{-1}$ rad$^{-2}$ during cooling and minimization, and set to 0 for the final molecular dynamics and energy minimization steps.

One hundred B3P models were generated starting from either a right-handed α-helix or an extended chain, and either of the 2 force fields described above, giving a total of 400 structures. Based on 89 distance restraints and 14 $\phi$ restraints, 30 ps of molecular dynamics simulation at 1000 K was followed by cooling to 100 K over a 15 ps period and energy minimization.

A second stage of simulated annealing included eight additional NOE restraints assigned by resolving ambiguous NOE interactions based on distances in the first-stage structures. Also, the intraresidue restraints between Y8 $H_{\epsilon 1+\epsilon 2}$ and either $H_\alpha$ or $H_N$ were redefined as very weak (1.8−6.0 Å) since the collective list of original restraint values was found to be incompatible with good geometry for Y8. It is likely that the observed intensities were enhanced by spin diffusion involving $H_\delta$ and $H_\epsilon$, although internal dynamics of bound B3P could also be a factor. No other NOE interactions were consistently violated in the first stage, so additional corrections for spin diffusion were not justified. Thirty picoseconds of molecular dynamics at 1000 K, with cooling to 100 K at a linear rate over a 15 ps period, was followed by additional molecular dynamics for 5 ps at 100 K that excluded $\phi$ angle restraint terms. Finally, all structures were subjected to 3500 steps of conjugate gradient minimization based on the CHARMM 22 force field including electrostatics and the refined NOE restraint list.

From the set of 400 B3P structures, a subset was selected for structural analysis based good geometry and few NOE violations. Approximately 80 structures were selected by having no NOE violations greater than 0.25 Å. This set was further reduced to 20 by eliminating those structures with any $\phi,\psi$ value in the disallowed regions of the Ramachandran plot (Gunasekaran et al., 1996; Kleywegt & Jones, 1996) specified with Procheck-NMR (Laskowski et al., 1996).

## RESULTS

*Enzyme Kinetics*. B3P was found to be a competitive inhibitor with the coenzyme, $NAD^+$, with $K_I$, the dissociation constant of B3P from G3PDH not bound to $NAD^+$, equal to 140 $\mu$M and $K_M$, the Michaelis−Menten constant for $NAD^+$, equal to 46 $\mu$M. The affinity of both band 3 and its cytoplasmic portion under similar conditions has been found to be higher with $K_I$ approximately $2.0 \times 10^{-8}$ M (Tsai et al., 1982). The peptide also exhibited mixed inhibition with the substrate analog, arsenate, with $K_{IC}$, the dissociation constant of B3P from G3PDH without arsenate bound, equal to 210 $\mu$M, $K_{IU}$, the dissociation constant of B3P from G3PDH with arsenate bound, equal to 500 $\mu$M, and $K_M$, the Michaelis−Menten constant for the substrate analog arsenate, equal to 27 $\mu$M. These types of inhibition of G3PDH were found for band 3 protein and the 23 kDa N-terminal fragment of band 3 (Steck et al., 1982), demonstrating that B3P binding is a good model for the interaction of band 3 with G3PDH.

When the dissociation rate, $k_{off}$, is much greater than the longitudinal magnetic relaxation and cross-relaxation, nuclear Overhauser effects are efficiently transferred between the bound state and the free state. Thus, the observed cross-relaxation is related to the bound-state cross-relaxation in a straightforward manner (Clore & Gronenborn, 1982). In the case of diffusion-limited binding, $k_{off}$ can be calculated as $K_d k_{on}$, where $k_{on}$ is the association rate and $K_d$ is the dissociation constant of B3P from G3PDH. $K_d$ was set to 140 $\mu$M, the competitive inhibition constant, $K_I$. (Using the highest affinity measured from the above kinetic studies gives the most conservative estimate for $k_{off}$.) Assuming a diffusion-limited value for $k_{on}$ of $10^8$ M$^{-1}$ s$^{-1}$ (Espenson, 1981), $k_{off}$ for B3P from G3PDH is calculated to be $1.4 \times 10^4$ s$^{-1}$. This rate is much greater than the cross-relaxation rates of 50 s$^{-1}$ estimated for proteins the size of G3PDH, safely putting this complex into the fast-exchange limit.

*Specificity of B3P Binding to G3PDH*. It is important to rule out the possibility of nonspecific binding of B3P at the high concentrations used for the ET-NOESY experiments (Murali et al., 1993, 1994). The predominance of specific binding is shown here by demonstrating competition between B3P and $NAD^+$ plus arsenate, the coenzyme and substrate analog for G3PDH, respectively. The longitudinal relaxation time, $T1$, the transverse relaxation time, $T2$, and the cross-relaxation time responsible for an NOE are mole fraction weighted averages between the free and bound states when a ligand is in fast-exchange. Thus, $T1$ and $T2$ values for B3P decrease upon the addition of G3PDH. Figure 1B illustrates how the addition of 0.125 mM G3PDH to 1.5 mM B3P broadens the relatively narrow resonances of free peptide, shown in Figure 1A. With the subsequent addition of 15 mM $NAD^+$ and 15 mM arsenate (Figure 1C), the resonances revert to within 10% of their original line widths, consistent with the relative affinities of the coenzyme and peptide for G3PDH. With respect to longitudinal relaxation, the B3P $T1$ values for $H_{\delta 1+\delta 2}$ and $H_{\epsilon 1+\epsilon 2}$ of Y8 decrease to 0.58 s in the presence of G3PDH, but revert back to that of the free peptide, 1.4 and 1.7 s for $H_{\delta 1+\delta 2}$ and $H_{\epsilon 1+\epsilon 2}$, respectively, upon addition of the coenzyme and substrate analog. Similarly, the significant NOE between $H_{\delta 1+\delta 2}$ and $H_{\epsilon 1+\epsilon 2}$ in the presence of enzyme reverts back to the negligible value of the free peptide when coenzyme and substrate are added. A 10:1 $NAD^+$:B3P ratio was necessary for these competition assays because the coenzyme binds allosterically and the $K_d$ values for coenzyme binding the third and fourth sites on G3PDH (Meunier & Dalziel, 1978)

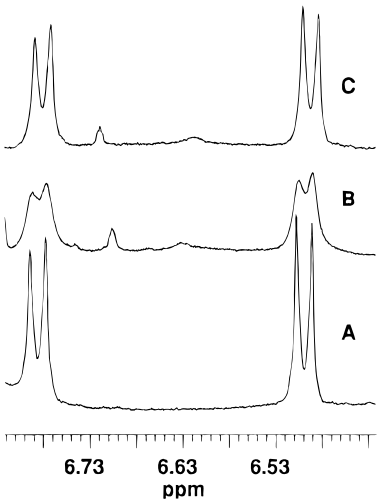


FIGURE 1: (A) 1D $^1$H NMR spectra showing the Y8 $H_{\delta1+\delta2}$ (6.79 ppm) and Y8 $H_{\epsilon1+\epsilon2}$ (6.50 ppm) resonances of 1.5 mM B3P in the free state, (B) in the presence of 0.125 mM G3PDH, and (C) in the presence of 0.125 mM G3PDH, 15.0 mM $NAD^+$, and 15.0 mM arsenate. Binding of B3P is specific, since the addition of coenzyme and arsenate, a substrate analog, reverses the broadening of B3P resonances that results from binding G3PDH. Samples contained 10 mM imidazole and 8 mM sodium acetate in 99.96% $D_2O$.

are nearly equal to the inhibition constant of the coenzyme−peptide complex. That the increase in ionic strength by addition of $NAD^+$ and arsenate weakens B3P binding (Mitchell et al., 1965) to produce the above effect was ruled out by adding 60 mM sodium acetate to give the same ionic strength as the samples shown in Figure 1C. The line widths of B3P and the NOE intensity between Y8 $H_{\delta1+\delta2}$ and Y8 $H_{\epsilon1+\epsilon2}$ do not revert back to those of the free peptide when acetate is added to the B3P−G3PDH complex.

Binding of B3P to concanavalin A, a tetramer at pH 7.5 (Chowdhury & Weiss, 1995), was probed in a similar fashion as binding to G3PDH to examine possible nonspecific binding by B3P to proteins in general at the high concentrations for NMR. The proton spectrum of 1.5 mM B3P and 0.125 mM concanavalin A in 99.96% $D_2O$, pH 7.5, was measured at 4 °C. Not only did the addition of this enzyme have little effect on B3P line widths, but no change was observed in either peptide $T1$ values or the NOE intensity between Y8 $H_{\delta1+\delta2}$ and Y8 $H_{\epsilon1+\epsilon2}$.

*Stoichiometry of the B3P−G3PDH Complex.* The B3P interaction with G3PDH was further characterized by determining the number of binding sites per G3PDH tetramer using Sephadex G-50 displacement chromatography (Penefsky, 1977) as described under Materials and Methods. From solutions of varying concentrations of B3P and G3PDH added to the column, the stoichiometry of the complex is determined from the limiting [B3P]:[G3PDH] ratio eluted off the column as a function of added [B3P]:[G3PDH] ratio (Figure 2). Measurement of the stoichiometry for B3P binding to G3PDH is complicated by residual coenzyme that copurifies with G3PDH since B3P competes with coenzyme for binding (described above). Coenzyme displays negative cooperativity for association with G3PDH and equals 10 nM for binding the highest affinity site (Meunier & Dalziel, 1978). Dialysis does not remove all of the bound coenzyme, as monitored by the ratio of absorbances at 280 and 260 nm (Vijlder & Slater, 1968; Fox & Dandliker, 1956), although part of the coenzyme remaining after dialysis can be removed

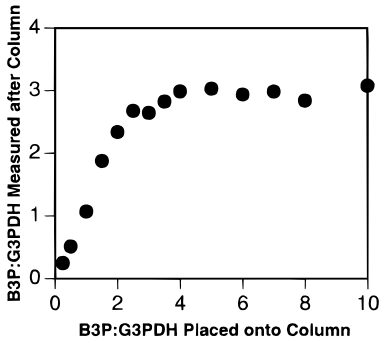


FIGURE 2: Sephadex G-50 displacement experiment of B3P and G3PDH prepared without charcoal treatment showing a stoichiometry of approximately three peptide molecules per enzyme tetramer when one G3PDH site is occupied by coenzyme (see text). The abscissa shows the varying B3P:G3PDH ratios added to the Sephadex G-50 column in 100 $\mu$L volumes. The ordinate shows the B3P:G3PDH ratios measured in the flow-through which contains the complex, while free peptide is retained on the column since the mobility of the ligand through the column is significantly slower.

by charcoal treatment. From the 280 nm:260 nm ratio, approximately 1.0−1.22 mol of coenzyme/mol of G3PDH remained after dialysis and approximately 0.50−0.72 mol of coenzyme/mol of G3PDH remained after charcoal treatment. Given the relative weaker affinity of B3P for G3PDH indicated by a $K_I$ of 140 $\mu$M, B3P is not expected to displace residual coenzyme at concentrations practical for these studies. As such, binding of B3P was measured using dialyzed G3PDH (associated with 1 mol of coenzyme) and charcoal-treated G3PDH (associated with 0.50−0.72 mol of coenzyme) to identify the influence of coenzyme binding on the apparent binding stoichiometry. Without charcoal treatment, the limiting B3P:G3PDH ratio off the column given by the plateau region in Figure 2 is approximately 3.0. In the case of charcoal-treated enzyme, the limiting ratio in the elution volume is 3.5 for addition of a 32:1 mole ratio to the column. Taken together, these results indicate that the binding stoichiometry for B3P is 4.0, or one B3P molecule per G3PDH subunit.

Work with human red cell ghosts and the cytoplasmic domain of band 3 has reported that band 3 binds the aldolase or G3PDH tetramer with a stoichiometry of 1:1 (Yu & Steck, 1975; Stapazon & Steck, 1977). That the N-terminal fragment, B3P, binds with a higher ratio, 4:1, to both G3PDH and aldolase (Schneider & Post, 1995) suggests steric hindrance as one reason for the reported differences in the stoichiometry of binding.

*Structure of B3P Bound to G3PDH from Transferred NOE Intensities.* The amide region of the ET-ssNOESY spectrum in Figure 3A shows transferred NOE cross-peaks for intramolecular B3P interactions. NOE interactions involving G3PDH protons are not observable because of their broad line widths. B3P was previously shown to have negligible NOE interactions in the unbound state (Schneider & Post, 1995). Thus, the intensities measured in the presence of G3PDH are a result from cross-relaxation in the bound state (Figure 3A,C). This point is illustrated by comparing NOESY spectra at 150 ms mixing time of B3P in the absence (Figure 3B) and presence (Figure 3C,D) of enzyme. Cross-peaks to Y8 $H_{\delta1+\delta2}$ and $H_{\epsilon1+\epsilon2}$ include only the fixed distance $H_\delta-H_\epsilon$ and one weak $H_\beta-H_\delta$ intraresidue NOE interactions in the free state, but in the presence of either G3PDH or

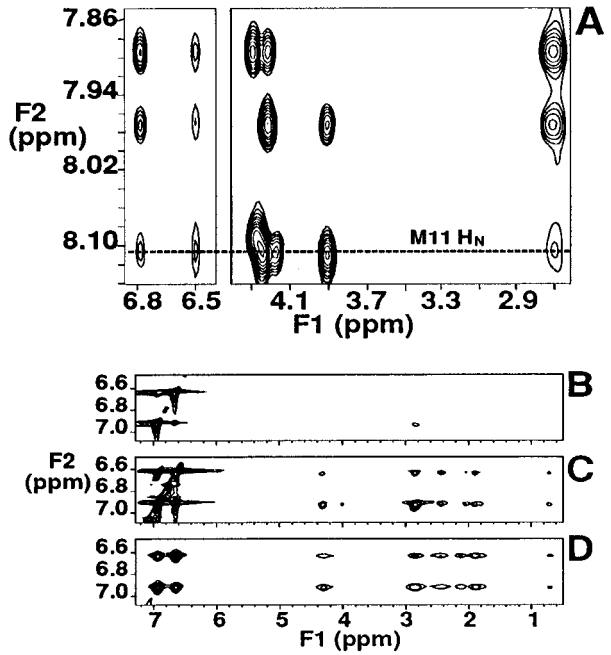


FIGURE 3: (A) Amide region of an ET-ssNOESY spectrum of 5.0 mM B3P with 0.125 mM G3PDH measured in 85% $H_2O$/15% $D_2O$ with a Varian UnityPlus 600 MHz spectrometer. The NOE interactions for M11 $H_N$ include the interresidue ones with Y8 $H_{\delta1,\delta2}$ (6.79 ppm), $H_{\epsilon1,\epsilon2}$ (6.5 ppm), and $H_{\beta1,\beta2}$ (2.69 ppm). (B) Aromatic region of 2D NOESY spectra measured on a Varian VXR-500 spectrometer of 5.0 mM B3P free, or (C) in the presence of 0.125 mM G3PDH, and (D) 2.8 mM B3P with 70 $\mu$M aldolase showing both the lack of NOE interactions with the free peptide (B) and the similarity of NOE interactions in the presence of either glycolytic enzyme (compare panel C with panel D). The Y8 $H_{\delta1,\delta2}$ and $H_{\epsilon1,\epsilon2}$ NOE interactions include L4 $H_{\delta1,\delta2}$ (0.55 ppm) and M12 $H_\epsilon$ (1.76 ppm). Spectra taken in the presence of G3PDH were collected at pH 7.5 and 4 °C with 10 mM imidazole and 8 mM sodium acetate, while those of B3P alone and in the presence of aldolase were collected at pH 5.5 and 25 °C with 10 mM phosphate. Gaussian apodization with zero-filling was used to generate 4K × 4K data matrices and a mixing time of 150 ms in all cases.

aldolase (Schneider & Post, 1995), a number of interresidue NOE interactions are found for the tyrosine ring. The intraresidue NOE interactions are also more intense in the presence of these glycolytic enzymes.

A total of 97 NOE interactions were interpreted from NOESY spectra in either $D_2O$ or 85% $H_2O$/15% $D_2O$. Of these, 54 were intraresidue interactions, 27 were sequential ($|i - j| = 1$), and 16 were nonsequential ($|i - j| > 1$) interresidue interactions (Table 1). With 37 NOE interactions, Y8 is the dominant residue contributing to the total number of NOE interactions.

Structure determination of B3P bound to G3PDH involved 14 $\phi$ dihedral restraints in the initial conformational search that were not included in the final steps, as described under Materials and Methods. As such, the dihedral restraints facilitate convergence starting from initial coordinates, but are not determinants of the final structures. The lack of bias from the $\phi$ restraints in the final 20 structures is evident in the Ramachandran plot in Figure 4A produced using Procheck-NMR (Laskowski et al., 1996). Protocols with either force field (see Materials and Methods) yielded structures having favorable van der Waals contacts and electrostatic interactions, resulting in half of the final 20 structures generated from each force field. Fifteen of these

Table 1: Comparison of B3P NOE Interactions When Bound to either G3PDH or Aldolase[a]

| | G3PDH | aldolase | G3PDH and aldolase | residues 4−9 for G3PDH and aldolase |
|---|---|---|---|---|
| NOEs | 97 | 68 | 46 | 29 |
| intraresidue | 54 | 37 | 27 | 17 |
| interresidue | 43 | 31 | 19 | 12 |
| $H_{\alpha,i}-H_{N,i+1}$ | 8 | 6 | 5[b] | 3 |
| >1 residue apart | 16 | 18 | 11[c] | 7 |
| $H_{\alpha,i}-H_{\alpha,i+1}$ | 0 | 1 | − | − |
| $H_{N,i}-H_{N,i+1}$ | 4 | 3 | 2[d] | 1 |

[a] Listed are the number of NOE interactions used to define B3P interproton distance restraints for simulated annealing and the number of NOE interactions observed for both G3PDH and aldolase complexes. [b] Cross-peaks between protons of residue 2 and 3, 3 and 4, 8 and 9, 9 and 10, and 14 and 15. [c] Cross-peaks between protons of residue 4 and 8 (4), 8 and 10, 8 and 12 (4), and 6 and 8 (2). [d] Cross-peaks between protons of residue 8 and 9, 13 and 14.

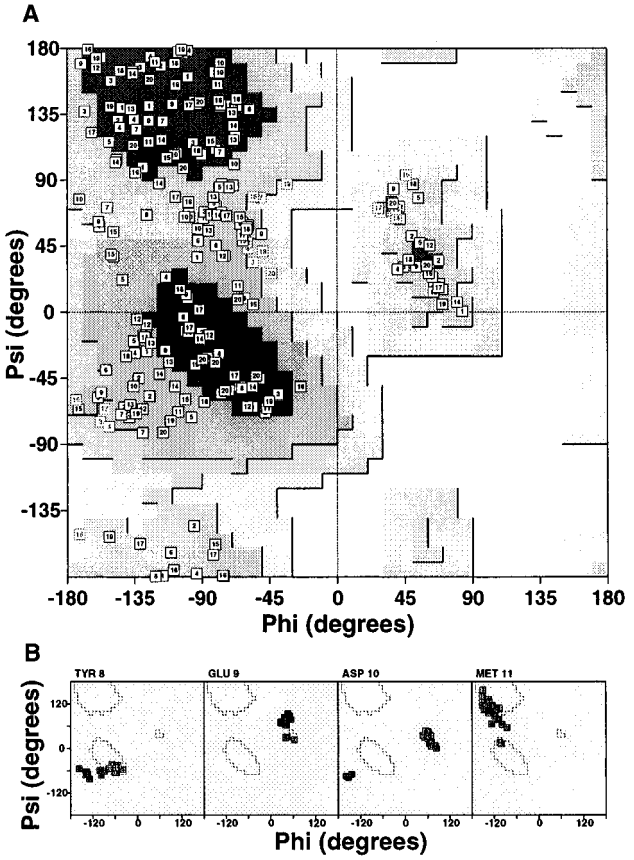


FIGURE 4: (A) Ramachandran plot containing all 20 selected B3P structures bound to G3PDH chosen from a set of 400 based on both low NOE violations and good geometry. (B) Individual residue Ramachandran plots of residues Y8 through M11 that form a $\beta$-turn for the 20 selected B3P structures. Plots were generated by Procheck-NMR (Laskowski et al., 1996).

structures started with an α-helix for the initial coordinates. The average total energy and NOE energy for the 20 structures were $-223 \pm 67$ kcal mol$^{-1}$ and $8.0 \pm 1.1$ kcal mol$^{-1}$, respectively. The average summed distance of violations per structure was $2.2 \pm 0.3$ Å, and the average number of NOE violations exceeding 0.2 Å was $2.0 \pm 0.8$ with a maximum violation of 0.25 Å.

The $C_\alpha$ trace for the 20 NMR structures is shown in Figure 5A. The average rmsd over the set of 20 for main-chain atoms (N, $C_\alpha$, and C) of residues 4 through 11 was 1.27 ±

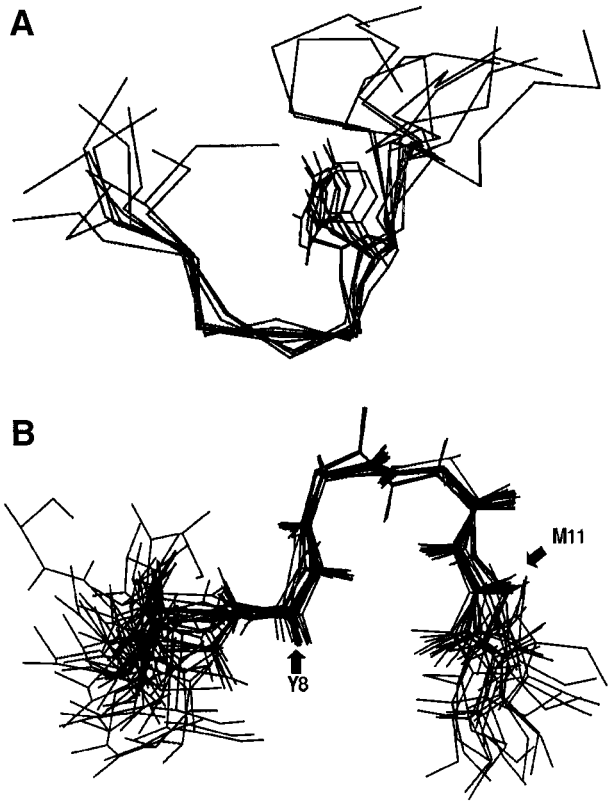


FIGURE 5: (A) $C_\alpha$ trace along with the side chain of Y8 from 10 of the final 20 selected structures of B3P (MEELQDDYEDM-MEEN-$NH_2$) bound to G3PDH. Main-chain atoms (N, $C_\alpha$, and C) of residues 4 through 9 were used to superimpose structures. (B) Backbone of residues 5 through 12 of the 20 selected B3P structures bound to G3PDH. Main-chain atoms of residues 8 through 11, a type IV $\beta$-turn, were used to superimpose the structures. This figure was generated with QUANTA (Molecular Simulations Inc.).

0.48 Å, while that for all main-chain atoms was 4.15 ± 1.20 Å, determined after a least-squares superposition of main-chain atoms for residues 4 though 11 and residues 1 through 15, respectively. These values illustrate the relatively good convergence in structure within the central residues of the peptide and the disorder among the termini. The PSI loop is stabilized intramolecularly through nonpolar interactions involving the triad of L4, Y8, and M12, and through a side-chain/side-chain hydrogen bond between Y8 and D10 (Figure 6A). These structural features are supported by the NOE interactions in Figure 3D (triad), and by the combined NOE interactions of E9 with Y8 and D10 (hydrogen bond). The relative spatial orientation of the side chains of L4, Y8, and M12 is maintained among the 20 structures in spite of the disordered structure of the terminal residues of B3P. This internal structure can be described by the triangle defined from three vectors joining L4, Y8, and M12: the distance L4 $C_\gamma$ to Y8 $C_\zeta$, L4 $C_\gamma$ to M12 $C_\epsilon$, and Y8 $C_\zeta$ to M12 $C_\epsilon$. The area of such a triangle is 9.97 ± 1.47 Å, showing small variation among the 20 structures. A $\beta$-turn terminates the PSI loop. The NOE interactions between the side-chain protons of Y8 and M11 $H_N$ (see Figure 3A) result in an average distance between Y8 $C_\alpha$ and M11 $C_\alpha$ of 6.0 ± 0.4 Å, and the $\phi,\psi$ angles from the 20 structures fall within a miscellaneous category termed type IV (Lewis et al., 1973; Wilmot & Thornton, 1988). The $\beta$-turn is well-defined (Figure 5B) with an rmsd of 0.39 ± 0.25 Å for main-chain atoms of residues 8 through 11. The distribution of $\phi,\psi$ values for the individual $\beta$-turn residues, Y8 through M11, is shown in Figure 4B. All but one of the values falling within the classical left-handed α-helix region are from residues E9 and D10.

*Comparison of B3P Bound to G3PDH and Aldolase*. The structures of B3P modeled from ET-NOESY data in the presence of either aldolase or G3PDH are similar. The comparison shown in Table 1 of the NOE interactions for B3P bound to either G3PDH or aldolase reveals the basis for this structural similarity. Out of 68 and 97 interactions for the aldolase and G3PDH complexes, respectively, 46 are observed in common. The majority of these, 29/46, involve residues 4 through 9. In addition, greater than half of the interresidue NOE interactions of the tyrosine ring (10/18) are common to both complexes. Many of the additional NOE interactions observed for the G3PDH complex, but not the aldolase complex, involve amide protons, which could be a consequence of a more efficient water suppression method in the ssNOESY experiment rather than an actual difference in the structures of bound B3P. The structural similarity in the PSI loop is shown in Figure 6C by superposition of main-chain atoms from residues 4 through 9 for five structures each of B3P determined for the G3PDH complex (green) and the aldolase complex (red) (Schneider & Post, 1995). The average rms pairwise difference in main-chain atoms (N,Cα, and C) for residues 4 through 9 using the 20 selected structures for each of the complexes (*i.e.*, 400 rms difference values) is 1.55 ± 0.39 Å. This average is slightly larger than the two averages, comparing residues 4 through 9, calculated within the set of NMR structures for one complex, which is 1.11 ± 0.40 Å for G3PDH and 1.21 ± 0.50 Å for aldolase. The ranges of rms pairwise differences for the 20 G3PDH structures, the 20 aldolase structures, and the comparison between the two sets are 0.07−1.91 Å, 0.25−2.18 Å, and 0.80−2.92 Å, respectively. The overlap of the ranges for comparison within a set of structures and between the two sets indicates similar structural solutions of B3P binding either G3PDH or aldolase. The side-chain interactions of the PSI loop are also comparable for the two glycolytic enzyme complexes of B3P. Comparison of B3P bound to G3PDH (Figure 6A) and to aldolase (Figure 6B) indicates that the nonpolar interactions of L4, Y8, and M12 stabilize both structures. We also note that the N and C termini are not converged in the NMR solutions for either complex. In the aldolase complex (Figure 6B), the tyrosine ring is sandwiched between L4 and M12, while in the G3PDH complex the ring is rotated, and the $\beta$-turn orients the main chain from residues 8 to 11 such that L4 and M12 lie on one side of the ring. The side-chain hydrogen bond between Y8 and D10, found for the G3PDH complex, occurs in some, but not all, of the aldolase-bound B3P structures. In the structural solutions for B3P bound to aldolase, the relative arrangement within the triad is more variable than that for G3PDH, due probably to the fewer amide distance restraints obtained for the B3P−aldolase complex. Fewer amide distance restraints may also be the reason no $\beta$-turn was found in the aldolase-bound structure of B3P, since the $\beta$-turn in the G3PDH complex is defined by NOE interactions involving M11 $H_N$.

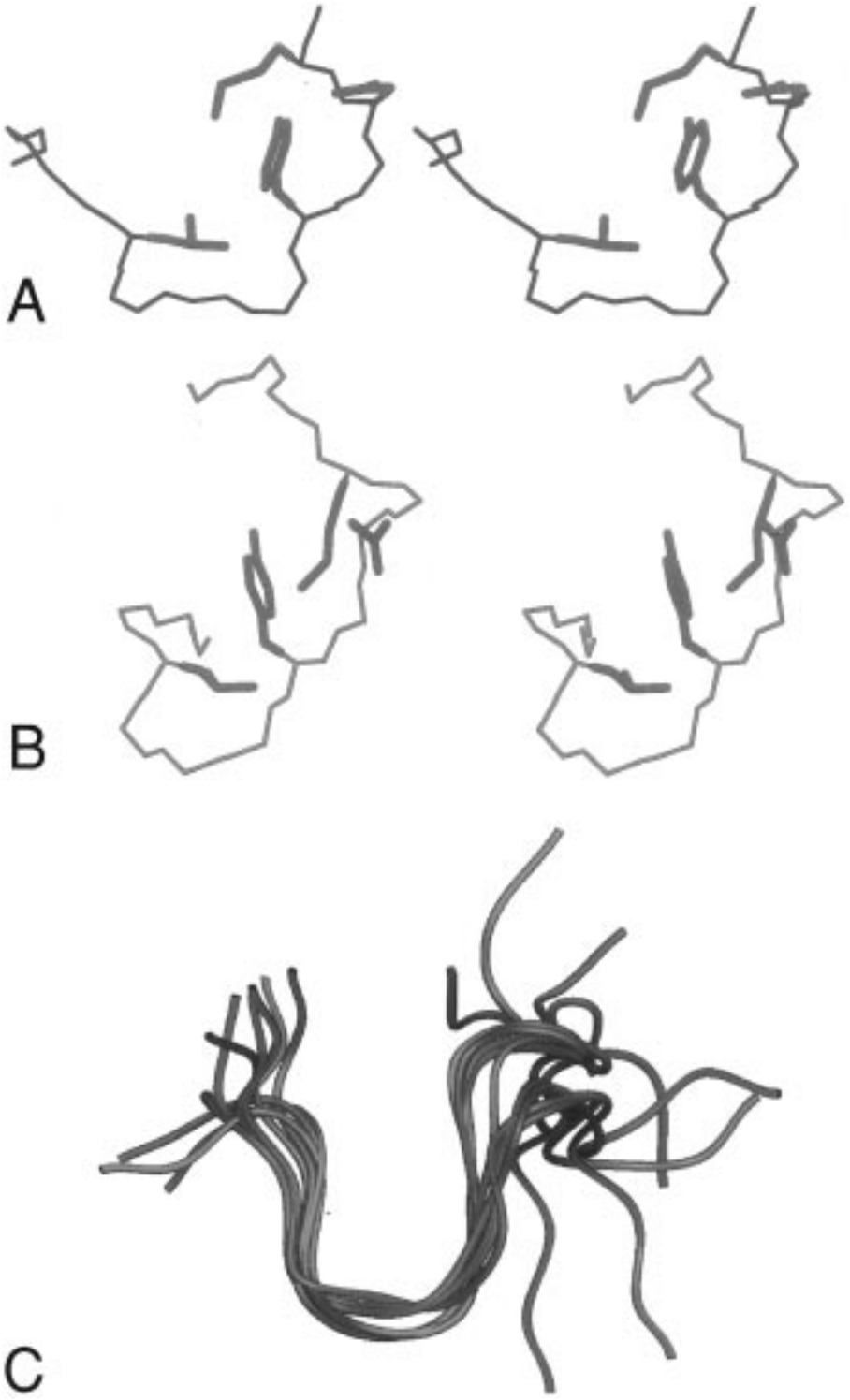


FIGURE 6: Stereoview of B3P main-chain plus residues that stabilize the PSI loop, L4, Y8, M12, and D10 for B3P bound to (A) G3PDH or to (B) aldolase. Shown in each case is 1 of the 20 structures that had low total energy and low NOE restraint energy. (C) Protein cartoon of five computed structures of B3P bound to either aldolase (red) or G3PDH (green), showing the similarity in the PSI loop recognized by both glycolytic enzymes. Main-chain atoms (N, $C_\alpha$, and C) of residues 4 through 9 were used to superimpose the structures. These figures were generated with QUANTA (Molecular Simulations Inc.).

## DISCUSSION

*PSI Loop of the B3P−G3PDH Complex.* The pentadecameric peptide, B3P, mimics the interaction of band 3 with G3PDH; B3P, the cytoplasmic domain of band 3, and full-length band 3 in erythrocyte ghost preparations all exhibit competitive inhibition against the coenzyme $NAD^+$ and noncompetitive inhibition against the substrate analog arsenate (this work; Tsai et al., 1982). The NMR studies reported here on the B3P−G3PDH complex, along with those on B3P−aldolase (Schneider & Post, 1996), elucidate certain structural features of the interaction between band 3 and the glycolytic enzymes and the disruption of this interaction upon tyrosine phosphorylation of band 3. We recognize that the complex formed by the larger cytoplasmic

domain of band 3 may involve features not contained within this peptide−protein model; however, structural information on the full protein−protein complex must await the difficult task of crystallization of a large molecular mass complex involving the cytoplasmic domain of band 3 (∼43 kDa) bound to a glycolytic enzyme (∼140 kDa).

Band 3 peptide binds to G3PDH in a PSI loop structure which, as a nonregular polypeptide structure, is well-defined by the NMR data. Residues 4−11 fold around Y8 (Figures 5 and 6) so that the nonpolar interactions of the L4, Y8, M12 triad and the Y8−D10 side-chain hydrogen bond stabilize the loop structure. The positions of D10 and M12 are linked to the type IV $\beta$-turn for residues 8−11 formed at the end of the PSI loop by residues 8 through 11. Calculation of the solvent-accessible surface shows that the tyrosine ring is buried and therefore not involved in intermolecular contacts.

A key finding by these studies is that B3P binds G3PDH and aldolase with a markedly similar structure, consistent with the high fraction of NOE interactions common to both complexes (Table 1). The main-chain fold for residues 4−11, forming the PSI loop, is nearly identical for B3P binding either to G3PDH (green in Figure 6C) or to aldolase (red in Figure 6C), and the nonpolar interactions of the triad L4, Y8, and M12 result in a similar internal structure of the loop (compare Figure 6A and Figure 6B). Importantly, the PSI loop structure reflects specific binding as shown by displacement of B3P by the enzymatic substrate or coenzyme (Schneider & Post, 1995; this work). It is useful to note that no evidence was found for the intrinsic structure of B3P free in solution.

*Tyrosine Phosphorylation Control of Protein−Protein Association.* Binding recognition and tyrosine phosphorylation control of protein−protein association based on the PSI loop differ from those involving SH2 or PTB domains of kinases and adapter proteins (Yu & Schreiber, 1994; Beattle, 1996; Harrison, 1996; Eck & Trub, 1996; Zhou et al., 1996). In the case of SH2 and PTB domains, phosphorylated tyrosine is required for binding, and the phosphotyrosine interacts directly with residues of the SH2 or PTB protein. In contrast, recognition of the PSI loop by glycolytic enzymes is for unphosphorylated tyrosine, with the tyrosine making only intramolecular contacts. In addition, a phosphopeptide binds to SH2 and PTB domains in a largely extended conformation, in contrast to the coiled structure of the PSI loop.

Phosphorylation of band 3 mediates against formation of the complex between band 3 and the glycolytic enzymes (Low et al., 1987; Harrison et al., 1991). The origin of this disruption by tyrosine phosphorylation is proposed to be intramolecular electrostatic repulsion based on the PSI loop structure (Schneider & Post, 1995). In the B3P−aldolase complex, the spatial proximity of the tyrosine hydroxyl group to carboxylates from Glu and Asp two to five residues removed from tyrosine means that tyrosine phosphorylation would destabilize the PSI loop structure by strong electrostatic repulsion. An analysis of the B3P structures for the G3PDH complex finds E3, D10, and E13 carboxyl groups at short distance to the Y8 hydroxyl group, consistent with this proposal. Moreover, the Y8−D10 hydrogen bond established for the B3P−G3PDH complex would be lost with tyrosine phosphorylation, further supporting a mechanism based on intramolecular destabilization for negative regulation of protein−protein association by tyrosine phosphorylation. Taken together, the factors described here for stabilization, and destabilization upon phosphorylation, lead to a plausible consensus for the PSI loop: -(D/E)LxxxYx-(D/E)xM(D/E)-.

*Binding Site for B3P.* The biochemical data are consistent with B3P binding within the active site of G3PDH or aldolase; for both complexes, the measured stoichiometry of binding is one B3P molecule per monomer, the enzyme kinetic data show competitive inhibition, and the displacement of B3P by substrates was demonstrated directly by NMR spectroscopy. For aldolase, the NMR structures of B3P were modeled in the active site using simulated annealing with NMR distance restraints for the peptide (Schneider & Post, 1995), and the strong steric and energetic complementarity between B3P and the active site in the resulting complexes are clearly consistent with active-site binding of B3P. The modeled complexes include a number of intermolecular hydrogen bonds involving acidic B3P residues with Lys and Arg residues of aldolase. In the case of G3PDH, crystallographic structures of lobster muscle G3PDH−coenzyme complex (Buehner, 1974; Harris & Waters, 1976) reveal R10 and K19 to be feasible candidates for interaction with acidic B3P residues. These G3PDH residues are in contact with the pyrophosphate moiety of $NAD^+$ and the phosphate moiety of the substrate. To determine that the active site of G3PDH can accommodate B3P sterically, and to assess the electrostatic complementarity with B3P, we visualized the NMR model for B3P in the context of the enzymatic active site using coordinates for G3PDH from human muscle (Watson & Campbell, 1972) (PDB entry 3GPD). Although the NMR structure has been determined here for B3P bound to G3PDH from rabbit muscle, G3PDH coordinates from this source are not available in the Brookhaven Protein data bank. The amino acid identity between G3PDH from these two sources is 90% according to the BLAST algorithm (Altschul et al., 1990), so that the assessment using the human muscle protein is reasonable. The active site of G3PDH is a crevice as wide as 20 Å, which can easily accommodate B3P spanning a maximum distance of approximately 15 Å. Furthermore, the conserved residues R10, K183, K191, and R231 (numbers refer to lobster muscle G3PDH) (Harris & Waters, 1976) form an electropositive surface that would provide a plausible binding region for the electronegative surface of B3P residues D6, D7, and E9. From the combination of the biochemical results and the structural considerations, we conclude that B3P binds to the active site of G3PDH.

## CONCLUSIONS

The structural similarity of B3P bound to G3PDH and aldolase underscores the importance of the PSI loop in the regulation of protein−protein association by tyrosine phosphorylation. The proposal made in this paper for negative control is based on the close intramolecular packing around tyrosine and obvious electrostatic destabilization that would result from tyrosine phosphorylation due to the proximity of several acidic residue side chains. Given the intramolecular nature of this mechanism for phosphorylation control, the question arises of whether a PSI loop might be involved in controlling protein−protein interactions other than that

between band 3 and the glycolytic enzymes. It is of interest, in this regard, to note that tyrosine phosphorylation mediates against association in downstream signaling events associated with cytoskeletal interactions (Balsamo et al., 1996; Behrens et al., 1993; Hamaguchi et al., 1993; Matsuyoshi et al., 1992; Takeda et al., 1995) and the control of microtubulin polymerization by microtubulin associated proteins (Wandosell et al., 1987).

## ACKNOWLEDGMENT

We thank Michael Schneider and Adam Zabell for their very helpful suggestions on every phase of this project; Tom Smith for his suggestions regarding chromatography; Dean V. Carlson and John F. Kozlowski for suggestions regarding NMR; William J. Ray, Jr., John Burgner II, and Joseph M. Puvathingal for suggestions regarding enzyme preparations and general biochemistry; and Marietta L. Harrison and P. S. Low for comments on the manuscript.

## SUPPORTING INFORMATION AVAILABLE

A table containing the $^1$H chemical shift assignments at pH 7.5 for B3P in the free state and the X-PLOR distance restraints file for B3P in the bound state (3 pages). Ordering information is given on any current masthead page.

## REFERENCES

Altschul, S. F., Gish, W., Miller, W., Myers, E. W., & Lipman, D. J. (1990) *J. Mol. Biol. 215*, 403−410.
Amelunxen, R. E. (1967) *Biochim. Biophys. Acta 139*, 2432.
Andreotti, A. H., Bunnell, S. C., Feng, S., Berg, L. J., & Schreiber, S. L. (1997) *Nature 385*, 93−97.
Balaram, P., Bothner-By, A. A., & Breslow, E. (1973) *Biochemistry 12*, 4695−4704.
Balsamo, J., Leung, T., Ernst, H., Zanin, M. K. B., Hoffman, S., & Lilien, J. (1996) *J. Cell Biol. 134*, 801−813.
Beattle, J. (1996) *Cell. Signalling 8*, 75−86.
Behrens, J., Vakaet, L., Friis, R., Winterhager, E., Van Roy, F., Mareel, M. M., & Birchmeier W. (1993) *J. Cell Biol. 120*, 757−766.
Bell, J. E., & Dalziel, K. (1975) *Biochim. Biophys. Acta 391*, 249−258.
Brooks, B. R., Bruccoleri, R. E., Olafson, B. D., States, D. J., Swaminathan, S., & Karplus, M. (1983) *J. Comput. Chem. 4*, 187−217.
Brunger, A. T. (1988) X-PLOR *Manual*, Yale University, New Haven, CT.
Brunger, A. T. (1992) *X-PLOR 3.1: A System for X-ray Crystallography and NMR*, Yale University Press, New Haven, CT.
Buehner, M., Ford, G. C., Moras, D., Olsen, K. W., & Rossmann, M., G. (1974) *J. Mol. Biol. 90*, 25−49.
Campbell, A. P., & Sykes, B. D. (1991) *J. Mol. Biol. 222*, 405−421.
Chowdbury, T. K., & Weiss, A. K. (1975) *Concanavalin A*, Plenum Press, New York.
Cleland, W. W. (1979) *Methods Enzymol. 63*, 103.
Clore, G. M., & Gronenborn, A. M. (1982) *J. Magn. Reson. 48*, 402−417.
Clore, G. M., & Gronenborn, A. M. (1983) *J. Magn. Reson. 53*, 423−442.
Conway, A., & Koshland, D. E. (1968) *Biochemistry 7*, 4011−4022.
Dekowski, S. A., Rybicki, A., & Drickamer, K. (1983) *J. Biol. Chem. 258*, 2750−2753.
De Vijlder, J. J. M., & Slater, E. C. (1968) *Biochim. Biophys. Acta 167*, 23−34.
Duggleby, R. G., & Dennis, D. T. (1974) *J. Biol. Chem. 249*, 167.
Eck, M. J., & Trub, T. (1996) *Cell 85*, 695−705.
Espenson, J. H. (1981) in *Chemical Kinetics and Reaction Mechanisms* (Espenson, J. H., Ed.) pp 168−170, McGraw-Hill Inc., New York.
Gamblin, S. J., Davies, G. J., Grimes, J. M., Jackson, R. M., Littlechile, J. A., & Watson, H. C. (1991) *J. Mol. Chem. 219*, 573−576.
Gunasekaran, K., Ramakrishnan, C., & Balaram, P. (1996) *J. Mol. Chem. 264*, 191−198.
Hamaguchi, M., Matsuyoshi, N., Ohnishi, Y., Gotoh, B., Takeichi, M., & Nagai, Y. (1993) *EMBO J. 12*, 307−314.
Harris, R. K. (1986) *Nuclear Magnetic Resonance Spectroscopy*, Wiley & Sons Publishers, New York.
Harris, J. I., & Waters, M. (1976) *The Enzymes*, pp 1−49, Academic Press, New York.
Harrison, M. L., Rathinavelu, P., Arese, P., Geahlen, R. L., & Low, P. S. (1991) *J. Biol. Chem. 266*, 4106−4111.
Harrison, M. L., Isaacson, C. C., Burg, D. L., Geahlen, R. L., & Low, P. S. (1994) *J. Biol. Chem. 269*, 955−959.
Harrison, S. C. (1996) *Cell 86*, 341−343.
Hoagland, V. D., Jr., & Teller, D. C. (1969) *Biochemistry 8*, 594−602.
Horecker, B. L., Tsolas, O., & Lai, C. Y. (1972) *The Enzymes* (*3rd Ed.*) *7*, 213−258.
Hubbard, S. R., Wei, L., Ellis, L., & Hendrickson, W. A. (1994) *Nature 372*, 746−754.
Iijima, H., Dunbar, J. B., Jr., & Marshall, G. R. (1987) *Proteins: Struct., Funct., Genet. 2*, 330−339.
Kaul, R. K., Prasanna Murphy, S. N., Reddy, A. G., Steck, T. L., & Kohler, H. (1983) *J. Biol. Chem. 258*, 7981−7990.
Kleywegt, G. J., & Jones T. A. (1996) *Structure 4*, 1395−1400.
Kliman, H. J., & Steck, T. L. (1980) *J. Biol. Chem. 256*, 6314−6321.
Kornberg, A., & Horecker, B. L. (1953) *Biochem. Prep. 3*, 23.
Kraulis, P. J., Clore, G. M., Nilges, M., Jones, T. A., Pettersson, G., Knowles, J., & Gronenborn, A. M. (1989) *Biochemistry 28*, 7241−7257.
Laskowski, R. A., Antoon, J., Rullmann, C., MacArthur, M. W., Kaptein, R., & Thornton, J. M. (1996) *J. Biomol. NMR 8*, 477−486.
Lewis, P. N., Momany, F. A., & Scheraga, H. A. (1973) *Biochim. Biophys. Acta 303*, 211−229.
Low, P. S. (1986) *Biochim. Biophys. Acta 864*, 145−167.
Low, P. S., Allen, D. P., Zioncheck, T. F., Chari, P., Willardson, B. M., & Geahlen, R. L. (1987) *J. Biol. Chem. 262*, 4592−4596.
Low, P. S., Rathinavelu, P., & Harrison, M. L. (1993) *J. Biol. Chem. 268*, 14627−14631.
MacKerell, A. D., Jr., Bashford, D., Bellott, M., Dunbrack, R. L., Jr., Field, M. J., Fischer, S., Gao, J., Guo, H., Ha, S., Joseph, D., Kuchnir, L., Kuczera, K., Lau, F. T. K., Mattos, C., Michnick, S., Ngo, T., Nguyen, D. T., Prodhom, B., Roux, B., Schlenkrich, M., Smith, J. C., Stote, R., Straub, J., Wiorkiewicz-Kuczera, J., & Karplus, M. (1992) *FASEB J. 6*, A143.
Matsuyoshi, N., Hamguchi, M., Taniguchi, S., Nagafuchi, A., Tsukita, S., & Takeichi, M. (1992) *J. Cell Biol. 118*, 703−714.
McDaniel, C. F., Kirtley, M. E., & Tanner, M. J. A. (1974) *J. Biol. Chem. 249*, 6478−6485.
Meunier, J. C., & Dalziel, K. (1978) *Eur. J. Biochem. 82*, 483−492.
Mitchell, C. D., Mitchell, W. B., & Hanahan, D. J. (1964) *Biochim. Biophys. Acta 104*, 348−358.
Murali, N., Jarori, G. K., Landy, S. B., & Nageswara Rao, B. D. (1993) *Biochemistry 32*, 12941−12948.
Murali, N., Jarori, G. K., & Nageswara Rao, B. D. (1994) *Biochemistry 33*, 14227−14236.
Neuhaus, D., & Williamson, M. (1989) *The Nuclear Overhauser Effect in Structural and Conformational Analysis*, VCH Publishers, Inc., New York.
Orsi, B. A., & Cleland, W. W. (1972) *Biochemistry 11*, 102−109.
Pawson, T. (1995) *Nature 373*, 573−580.
Penefsky, H. S. (1977) *J. Biol. Chem. 252*, 2891−2899.
Prasanna Murthy, S. N., Liu, T., Kaul, R. K., Kohler, H., & Steck, T. L. (1981) *J. Biol. Chem. 256*, 11203−11209.
Schneider, M. L., & Post, C. B. (1995) *Biochemistry 34*, 16574−16584.
Sicheri, F., Moarefi, I., & Kuriyan, J. (1997) *Nature 385*, 602−606.
Sklenar, V., & Bax, A. (1987) *J. Magn. Reson. 74*, 469−479.

Smallcombe, S. H. (1992) *J. Am. Chem. Soc. 115*, 4776−4785.
Soukri, A., Mougin, A., Corbier, C., Wonacott, A., Branlant, C., & Branlant, G. (1989) *Biochemistry 28*, 2586−2592.
Stapazon, E., & Steck, T. L. (1977) *Biochemistry 16*, 2966−2971.
Takeda, H., Nagafuchi, A., Yonemura, S., Tsukita, S., Behrens, J., Birchmeier, W., & Tsukita, S. (1995) *J. Cell Biol. 131*, 1839−1847.
Tsai, I., Prasanna Murthy, S. N., & Steck, T. L. (1982) *J. Biol. Chem. 257*, 1438−1442.
Tuy, F. P. D., Henry, J., Rosenfeld, C., & Kahn, A. (1983) *Nature 305*, 435−438.
Tuy, F. P. D., Henry, J., & Kahn, A. (1985) *Biochem. Biophys. Res. Commun. 126*, 304−312.
Van Schaik, R. C., Berendsen, H. J. C., Torda, A. E., & Van Gunsteren, W. F. (1993) *J. Mol. Biol. 234*, 751−762.
Wandosell, F., Serrano, L., & Avila, J. (1987) *J. Biol. Chem. 262*, 8268−8273.
Watson, H. C., Duee, E., & Mercer, W. D. (1972) *Nature (London), New Biol. 240*, 130−133.
Wilmot, C. M., & Thornton, J. M. (1988) *J. Mol. Biol. 203*, 221−232.
Wüthrich, K. (1986) *NMR of Proteins and Nucleic Acids*, Wiley & Sons Publishers, New York.
Xu, W., Harrison, S. C., & Eck, M. J. (1997) *Nature 385*, 595−601.
Yannoukakos, D., Corinne, V., Piau, J. P., Wajcman, H., & Bursaux, E. (1991) *Biochim. Biophys. Acta 1061*, 253−266.
Yu, H., & Schreiber, S. L. (1994) *Struct. Biol. 7*, 417−420.
Yu, W., & Steck, T. L. (1975) *J. Biol. Chem. 250*, 9176−9184.
Zheng, J., & Post, C. B. (1993) *J. Magn. Reson. 101*, 262−270.
Zhou, M.-M., Huang, B., Olejniczak, E. T., Meadows, R. P., Shuker, S. B., Miyazaki, M., Trub, T., Shoelson, S. E., & Fesik, S. W. (1996) *Nat. Struct. Biol. 3*, 388−393.

BI971445B